J. Synchrotron Rad. (1998). **5**, 376–378

Submicrometre resolution phase-contrast radiography with the beam from an X-ray waveguide

S. Di Fonzo,[a]* W. Jark,[a] G. Soullié,[a] A. Cedola,[b,c] S. Lagomarsino,[d] P. Cloetens[c,e] and C. Riekel[c]

[a]Sincrotrone Trieste, SS14 Km 163.5, Area Science Park, 34012 Basovizza, Trieste, Italy, [b]INFM, Corso Perrone 24, 16152 Genova, Italy, [c]ESRF, BP 220, F-38043 Grenoble CEDEX, France, [d]Istituto di Elettronica dello Stato Solido (IESS), CNR, V. Cineto Romano 42, 00156 Roma, Italy, and [e]EMAT, University of Antwerp (RUCA), B-2020 Antwerp, Belgium. E-mail: difonzo@elettra.trieste.it

(*Received 4 August 1997; accepted 11 December 1997*)

Experimental data with unprecedented submicrometre resolution obtained in a phase-contrast radiography experiment in a magnifying configuration are presented. The term 'phase contrast' here indicates that the phase retardation of coherent light in matter was utilized as the contrast mechanism. The coherent and divergent beam exiting an X-ray waveguide was used in a lensless configuration to magnify spatial variations in optical path length up to several hundred times. The defocused image of a nylon fibre was measured with a resolution of 0.14 μm at the object. Sufficient contrast was found for exposure times of 0.1 s, *i.e.* in the regime for real-time studies.

Keywords: X-ray phase contrast; X-ray waveguides; projection microscopy; high-resolution imaging; resonant beam couplers.

1. Introduction

Traditional X-ray imaging techniques such as radiography and tomography rely on the variation of the absorption coefficient for X-rays in different materials as the origin of the contrast detected in the images. With increasing photon energy and especially in low-density materials, such as carbon-based or biological samples, the attenuation in the sample often becomes so small that no reasonable contrast can be obtained. Instead, phase-contrast radiography, which makes use of the phase modulation induced by an object in a coherent beam as the contrast mechanism, will still allow one to investigate the sample structure (see *e.g.* Davis *et al.*, 1995; Snigirev *et al.*, 1995; Cloetens *et al.*, 1996, 1997).

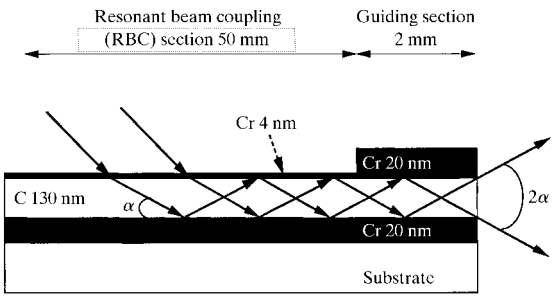

Figure 1
Cross section of the X-ray waveguide used for this investigation.

Recently the propagation of highly collimated coherent radiation was used in a lensless transmission geometry to convert phase modulations in intensity modulations. The absence of magnification limits the resolution to the detector resolution, *i.e.* ∼1 μm in the best case. Here we are describing another lensless set-up which uses the coherent and divergent beam exiting an X-ray waveguide in a projection-imaging configuration. Indeed, the configuration very much resembles that of an in-line holography experiment (Gabor, 1948). The submicrometre source size and the magnification in the scheme allow us to achieve submicrometre resolution without any severe demand on the detector resolution.

2. Experiment

The 'condenser' system in the presented projection microscope is formed by an X-ray waveguide (Feng *et al.*, 1995; Lagomarsino *et al.*, 1996; Jark *et al.*, 1996), as presented in Fig. 1. The object is a thin-film resonator, which has a layer of a low-absorbing material (C) enclosed between two metal layers (Cr) with smaller refractive index. These layers were produced at the Sincrotrone Trieste by low-pressure sputter coating onto ultrasmooth plane zerodur mirrors. For particular angles of grazing incidence the incident intensity can be coupled in a resonant manner to standing waves in the resonator. In this set-up the beam is compressed with the subsequent intensity enhancement, however, only in one direction. Finally, the trapped wave emerges from the end of the waveguide with higher intensity than a simple slit with the same thickness as the resonator would provide. While the coupling section has a semitransparent metal cover, a guiding section to the waveguide terminal has an opaque cover, so that no leakage intensity will interfere with the exiting intensity. After leaving the waveguide in the plane of beam compression, the wave has a divergence of about 0.7 mrad and it is highly coherent (Jark *et al.*, 1996). With the latter property the resolution obtainable in an imaging experiment is no longer limited to the beam size at the waveguide exit, as would be the case for an incoherent source.

The experimental configuration is shown in Fig. 2. Besides the waveguide, only a sample and a two-dimensional detector are needed. For the latter we used a low-noise fast-readout CCD

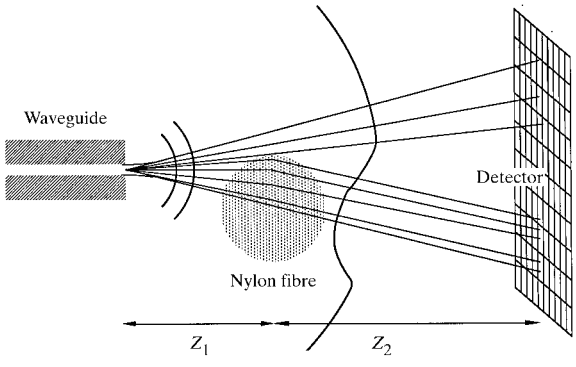

Figure 2
Schematic illustration of the hard X-ray magnifying set-up. A waveguide delivers a coherent and divergent beam which is transmitted through the sample (at the distance Z_1 from the waveguide) and propagates from there a distance Z_2 towards the position-sensitive detector. While the wavefronts are almost perfectly spherical at the position of the sample (emitted by a point source coincident with the exit of the waveguide), they are distorted behind the object.

camera (Labiche *et al.*, 1996) with an X-ray converter and light optics adjusted such that a pixel corresponded to a square of side 6.5 μm.

The experiment was carried out at the microfocus beamline (ID13) at the European Synchrotron Radiation Facility (ESRF), with an unfocused 13 keV beam from an Si (111) channel-cut monochromator and with the experimental set-up operated in air. The waveguide–sample distance, Z_1, could be as small as ~0.1 mm; here it was adjusted to 4.1 mm. A piezoelectric transducer with a resolution better than 0.1 μm was used to scan the sample through the beam. The X-ray converter screen of the CCD camera was positioned at a distance $Z_1 + Z_2 = 0.99$ m from the end of the waveguide, resulting in a magnification factor of 241. Fig. 3 shows the intensity distribution measured for a nylon fibre of diameter 12 μm. The vertical beam size of approximately 3 μm at the sample position was insufficient to illuminate the whole fibre. Fig. 3 is thus the combination of several images which were obtained in a vertical sample scan and scaled to the incident intensity. The latter procedure served to correct for the non-uniform beam intensity. In Fig. 3 it is obvious that one edge of the fibre is straight, as expected, while the other edge is deformed due to damage in this region, as was found later by an inspection in a scanning electron microscope. For this reason only the perfect edge was analysed further. The intensity distribution at this edge integrated over all pixels is presented in Figs. 4(*a*)–4(*c*) as experimental points.

3. Discussion

The recorded image is not a simple magnified image of the object, but a hologram created by a superposition of the undisturbed beam and the waves diffracted by the object. This is very similar to in-line holography in classical optics and to a defocused image in high-resolution electron microscopy. The field at the level of the detector can be expressed in the Fresnel approximation as the convolution of an object transmission function, taking into account the internal sample structure, and the free-space propagation function (Cloetens *et al.*, 1996; Wilkins *et al.*, 1996), which depends on the defocusing distance $D = Z_1Z_2/(Z_1 + Z_2)$. Here Z_1 and Z_2 indicate, as shown in Fig. 2, the source–object and object–detector distances, respectively. Described in other words, the measured hologram is a magnification of the corresponding Fresnel diffraction pattern obtained at a propagation distance D with plane-wave illumination. The magnification is simply given by $M = (Z_1 + Z_2)/Z_1$.

The focused image (at $D = 0$) is only sensitive to the absorption in the sample and thus corresponds to a conventional (absorption contrast) radiograph. Effects in the defocused image due to the finite field of illumination of the sample can be taken into account by an appropriate window function superimposed onto the sample transmission function. A finite resolution function of Gaussian shape will account for experimental limitations like vibrations, detector resolution or a limited source size. The latter is not very important here because of the use of a highly coherent source.

The modulation depth of the simulated intensity distribution at a fibre edge depends very strongly on the resolution functions as is evident in the simulations in Figs. 4(*a*)–4(*c*). These simulations of the experimental data followed the above-described scheme with the nylon fibre parameters and resolution functions of Gaussian shape with full width at half-maximum (FWHM) of 0, 0.15 and 0.3 μm. The comparison of the measured data with the simulations indicates that the measurement was made with a resolution of between 0.1 and 0.2 μm. This result is confirmed with a more reliable value of 0.14 μm by measurements under the

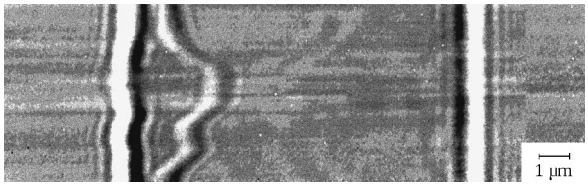

Figure 3
Phase-contrast image of a 12 μm-thick nylon fibre for $Z_1 = 4.1$ mm and $Z_2 = 986$ mm ($M = 241$) at an X-ray energy of 13 keV (fibre axis is vertically oriented). The figure is the superposition of different images recorded in a scan across the fibre (here the horizontal direction). Fresnel diffraction fringes are visible only close to the edges of the fibre.

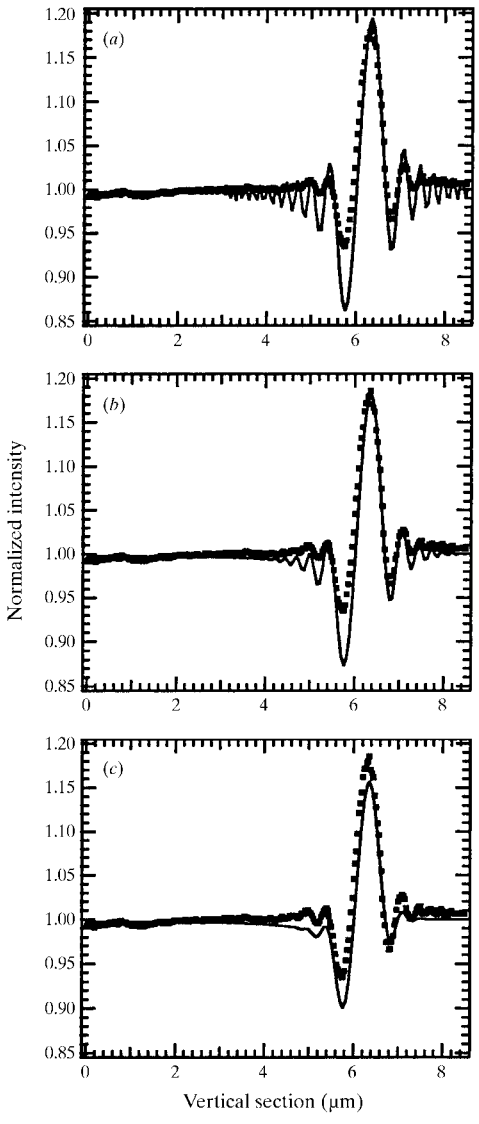

Figure 4
Comparison of the experimental horizontal intensity distribution (starting at the fibre centre) across the perfect edge of Fig. 3 integrated in the vertical direction over all pixels with simulations. They are made using the procedure discussed in the text for the structural parameters of the fibre as obtained from scanning electron microscopy (SEM) images and for three different values for the spatial resolution: (*a*) 0 μm, (*b*) 0.15 μm, (*c*) 0.3 μm.

same experimental conditions of a periodic bar pattern consisting of five submicrometre-sized gold bars (Lagomarsino *et al.*, 1997). The experiment was affected by a significant noise and vibration level close to the sample. A reduction of the disturbances improved the resolution from 0.2 μm to the reported 0.14 μm obtained with still recognizable vibrations. With the latter observation we attribute the limited resolution mainly to the residual vibrations in our set-up, even though its agreement with the resonator thickness would favour an explanation as a source size limit.

The good quality of the data will allow reconstruction of the transmission function based on an adapted numerical algorithm (Coene *et al.*, 1992) with the above-indicated spatial resolution. This investigation is presently underway.

4. Conclusions

We have shown that in magnifying phase-contrast radiography experiments, by use of the divergent and coherent beam exiting an X-ray waveguide, submicrometre resolution can be obtained with a detector of moderate resolution. The observed contrast originates from variations in the optical path length (*i.e.* a variation of the phase retardation) which is strongest in the vicinity of abrupt changes in sample density (*e.g.* edges). This allows one to study the internal structure of weakly absorbing and biological material in a non-destructive experiment in air. As exposure times of fractions of a second gave sufficient contrast, even dynamical processes are candidates to be studied at high-brightness third-generation synchrotron radiation sources. A spatial resolution of 0.14 μm was achieved in the defocused images; however, with better vibration isolation a smaller value should be obtainable. The reported resolution was achieved in only one direction; however, work on focusing in the other direction is underway.

References

Cloetens, P., Barrett, R., Baruchel, J., Guigay, J. P. & Schlenker, M. (1996). *J. Phys. D*, **29**, 133–146.
Cloetens, P., Pateyron-Salome, M., Buffiere, J. Y., Peix, G., Baruchel, J., Peyrin, F. & Schlenker, M. (1997). *J. Appl. Phys.* **81**, 5878–5884.
Coene, W., Janssen, A., Op de Beeck, M. & Van Dyck, D. (1992). *Phys. Rev. Lett.* **69**, 3743–3746.
Davis, T. J., Gao, D., Gureyev, T. E., Stevenson, A. W. & Wilkins, S. W. (1995). *Nature (London)*, **373**, 595–598.
Feng, Y. P., Sinha, S. K., Fullerton, E. E., Grübel, G., Abernathy, D., Siddons, D. P. & Hastings, J. B. (1995). *Appl. Phys. Lett.* **670**, 3647.
Gabor, D. (1948). *Nature (London)*, **161**, 777–778.
Jark, W., Di Fonzo, S., Lagomarsino, S., Cedola, A., Di Fabrizio, E., Brahm, A. & Riekel, C. (1996). *J. Appl. Phys.* **80**, 4831–4836.
Labiche, J. C., Segura-Puchades, D., Van Brussel, D. & Moy, J. P. (1996). *ESRF Newsl.* **25**, 41–43.
Lagomarsino, S., Cedola, A., Cloetens, P., Di Fonzo, S., Jark, W., Soullie, G. & Riekel, C. (1997). *Appl. Phys. Lett.* **71**, 2557–2559.
Lagomarsino, S., Jark, W., Di Fonzo, S., Cedola, A., Mueller, B., Engstrom, P. & Riekel, C. (1996). *J. Appl. Phys.* **79**, 4471–4473.
Snigirev, A., Snigireva, I., Kohn, V., Kuznetsov, S. & Schelokov, I. (1995). *Rev. Sci. Instrum.* **66**, 5486–5492.
Wilkins, S. W., Gureyev, T. E., Gao, D., Pogany, A. & Stevenson, A. W. (1996). *Nature (London)*, **384**, 335–338.